Convectively Driven Mixing in the Bottom Boundary Layer

J. N. Moum, A. Perlin, J. M. Klymak, M. D. Levine, T. Boyd, and P. M. Kosro

College of Oceanic and Atmospheric Sciences, Oregon State University, Corvallis, Oregon

(Manuscript received 15 September 2003, in final form 6 April 2004)

ABSTRACT

Closely spaced vertical profiles through the bottom boundary layer over a sloping continental shelf during relaxation from coastal upwelling reveal structure that is consistent with convectively driven mixing. Parcels of fluid were observed adjacent to the bottom that were warm (by several millikelvin) relative to fluid immediately above. On average, the vertical gradient of potential temperature in the superadiabatic (statically unstable) bottom layer was found to be -1.7×10^{-4} K m^{-1}, or 6.0×10^{-5} kg m^{-4} in potential density. Turbulent dissipation rates (ε) increased toward the bottom but were relatively constant over the dimensionless depth range 0.4–1.0z/D (where D is the mixed layer height). The Rayleigh number Ra associated with buoyancy anomalies in the bottom mixed layer is estimated to be approximately 10^{11}, much larger than the value of approximately 10^{3} required to initiate convection in simple laboratory or numerical experiments. An evaluation of the data in which the bottom boundary layer was unstably stratified indicates that the greater the buoyancy anomaly is, the greater the turbulent dissipation rate in the neutral layer away from the bottom will be. The vertical structures of averaged profiles of potential density, potential temperature, and turbulent dissipation rate versus nondimensional depth are similar to their distinctive structure in the upper ocean during convection. Nearby moored observations indicate that periods of static instability near the bottom follow events of northward flow and local fluid warming by lateral advection. The rate of local fluid warming is consistent with several estimates of offshore buoyancy transport near the bottom. It is suggested that the concentration of offshore Ekman transport near the bottom of the Ekman layer when the flow atop the layer is northward can provide the differential transport of buoyant bottom fluid when the density in the bottom boundary layer decreases up the slope.

1. Introduction

An important asymmetry in the nature of the bottom boundary layer (BBL) over a sloping bottom appears in observations (Hosegood and van Haren 2003; Lentz and Trowbridge 1991; Weatherly and Martin 1978) and numerical experiments (Trowbridge and Lentz 1991; MacCready and Rhines 1993). In particular, the bottom mixed layer is observed to be thicker during coastal downwelling than during upwelling. As well, indirect evidence from moored observations indicates enhanced turbulence during downwelling relative to upwelling (Hosegood and van Haren 2003). Model results indicate this asymmetry is associated with the cross-slope Ekman transport of buoyancy along the bottom. During upwelling, the advance of dense fluid up the slope increases the total stratification in the water column and limits vertical mixing to a thin bottom boundary layer. During downwelling, the motion is reversed, resulting in weakened stratification and a thickened bottom mixed layer. Models suggest the possibility of gravitational instability as the source of enhanced mixing in the BBL, leading to thickened bottom mixed layers, but the details of this process have not been observed until recently. In this paper, we examine observations from an intensive field experiment over the continental shelf off Oregon in which near-bottom vertical mixing during coastal downwelling is driven by active convection over a large cross-shelf extent of the BBL.

Convectively driven mixing is a consequence of the static instability resulting from relatively dense fluid lying above lighter fluid. It is a common feature of the daytime atmospheric boundary layer, in which the atmosphere is heated from below (Stull 1988; Caughey and Palmer 1979) and of the nighttime oceanic boundary layer, in which the ocean surface is cooled by the atmosphere above (Shay and Gregg 1986; Anis and Moum 1992; Soloviev and Klinger 2001). Nighttime convection in the upper ocean at midlatitudes may extend vertically to 100 m or so.

The process of convection involves buoyant parcels of fluid that rise (or fall, in the case of negative buoyancy—i.e., cooling from above) as their buoyancy exceeds opposing viscous forces. The comparative strengths of these forces is related through the Rayleigh number Ra. When Ra is sufficiently large, buoyant parcels (or thermal plumes) form, which appear to occur intermittently in space and time. This intermittency can

Corresponding author address: J. N. Moum, College of Oceanic and Atmospheric Sciences, Oregon State University, 104 Ocean Admin. Bldg., Corvallis, OR 97331-5503.
E-mail: moum@coas.oregonstate.edu

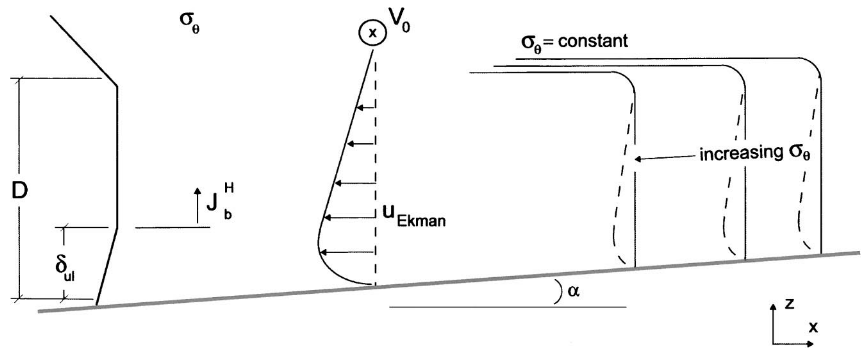

FIG. 1. Schematic diagram that indicates the structure of potential density (σ_θ) and velocity above a bottom sloping upward (slope α) to the east at a time when the current atop the Ekman layer flows northward (at speed V_0) and the density of the fluid in the bottom boundary layer decreases up the slope. On the profile of σ_θ at left are defined the height of the bottom mixed layer D and the thickness of the unstable layer δ_{ul} adjacent to the bottom and the neutral layer immediately above. The buoyancy flux into the neutral layer is J_b^H. A profile of the offshore component of the velocity in the Ekman layer is denoted u_{Ekman}. The consequence of this velocity profile to isopycnals with initial state indicated with black lines (to the right above) is suggested by the dashed lines.

be seen in numerical simulations of convectively driven mixing in the upper ocean (Skyllingstad and Denbo 1995). Good observations of the kinematics of this process are difficult to make in geophysical fluids. However, there are a certain number of distinguishing characteristics that have been determined from averaged vertical profiles through convectively mixed layers. These characteristics are common to both ocean and atmosphere and include

1) a superadiabatic (unstable) potential temperature gradient at the boundary,
2) a well-mixed layer away from the boundary, and,
3) in the mixed layer away from the boundary, a balance between the turbulent kinetic energy dissipation rate ε and the buoyancy flux.

These characteristics are summarized by Shay and Gregg (1986), Imberger (1985), Brubaker (1987), Lombardo and Gregg (1989), and Anis and Moum (1992, 1994) for the upper ocean during periods of surface cooling. The analogous conditions for the atmosphere during surface heating are discussed by Stull (1988) and Caughey and Palmer (1979).

A schematic of the structure of the density profile in a convectively driven boundary layer is shown in Fig. 1. The mixed layer height D is defined from density profiles (Perlin et al. 2004b, manuscript submitted to *J. Geophys. Res.*, hereinafter PMK) as the distance from the bottom over which the potential density σ_θ decreases by 0.0006 kg m^{-3} from its bottom value (the bottom value is determined by the vertical average over the bottom 10 cm).[1] The sum of unstable layer thickness (δ_{ul}) plus neutral layer thickness is almost equal to but slightly less than D. The difference between D and the sum of neutral plus unstable layers is the slight incursion into the stable layer above the mixed layer that results from the definition of D.[2]

Here, we use the two sets of terms, mixed/neutral layer and superadiabatic/unstable layer, interchangeably. A neutrally stable layer is defined to be mixed in density, and the interchangeable use of these two adjectives is justified. However, the use of the term unstable for superadiabatic is not quite correct. The term superadiabatic strictly refers to potential temperature decreasing with height. So far as potential density is determined by potential temperature, the profile is statically unstable. The condition for instability, though, is related through Ra (section 5), which includes the effects of viscosity and thermal diffusion. We follow atmospheric terminology in referring to the superadiabatic layer as an unstable layer.

In the spring of 2001, we repeated a sequence of transects at the same location across the continental shelf off Oregon (Fig. 2). The period of observations included two clear upwelling events bounding a period of reduced and reversed winds and subsequent relaxation from upwelling to downwelling conditions (PMK). Our observations include measurements of turbulence and density through the BBL. In this paper we use an analysis of these observations to illustrate the process of convective mixing in the BBL. In the example presented here the source of buoyancy flux is lateral advection, yet the process is clearly analogous to one-dimensional atmospherically forced convection in the upper ocean.

[1] The value of 0.0006 kg m^{-3} is sufficiently large in comparison with the precision of our density estimate yet small enough to clearly define D based on visual comparison with hundreds of individual density profiles. A further criterion, that 50 successive 2-cm bins are smaller than the bottom value by 0.0006 kg m^{-3}, effectively permits turbulent overturns within D.

[2] In the terminology applied to the convectively driven atmospheric boundary layer, the unstable layer is referred to as the surface layer and the neutral layer as the mixed layer. For the ocean, we have traditionally referred to the sum of these as the mixed layer.

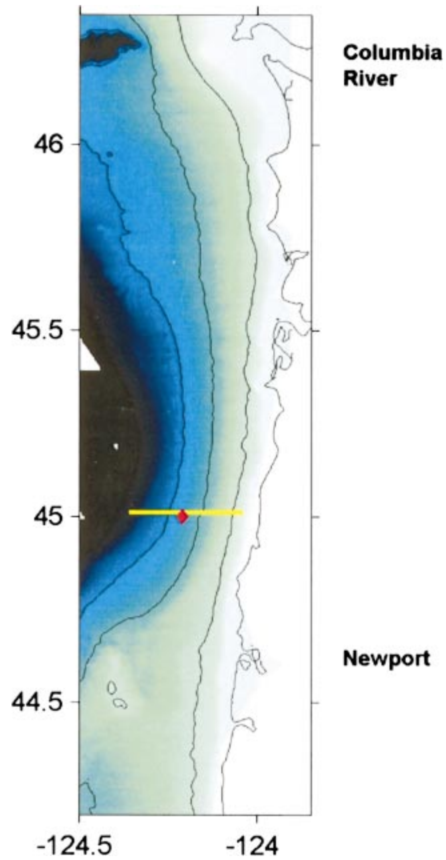

FIG. 2. Location of the experiment off the Oregon coast. Cross-shelf range of repeated transects is shown in yellow. The mooring location is shown as a red diamond. Depths are contoured at 50, 100, and 150 m.

2. Profile observations

Profiling measurements were made using our freely falling turbulence profiler, Chameleon (Moum et al. 1995). Chameleon was deployed from the fantail of the R/V *Thomas G. Thompson.* Measurements were made of small-scale temperature and conductivity as well as of velocity gradients, from which the viscous rate of dissipation of turbulent kinetic energy ε was estimated using the method described by Moum et al. (1995). For this experiment, Chameleon was outfitted with a ring to protect the nose sensors from destruction upon impact with the bottom. This modification permitted us to profile through the BBL to within a few centimeters of the bottom.[3]

The observations discussed here are 4 (of 12) rapidly repeated transects in May of 2001 across the continental shelf off Oregon (at 45°02′N). Transects extend to 25 km offshore from the 30-m depth contour (Fig. 2). These observations have provided a detailed view of the cross-shelf motion of the BBL in response to variations in direction and intensity of alongshore winds (PMK). Dense BBL fluid was drawn up the shelf in accord with Ekman dynamics. Upon relaxation from upwelling winds, the dense bottom fluid retreated back down the shelf. At the same time, the BBL thickened and was observed to be highly turbulent.

A sequence of transects that illustrate the BBL's response to a relaxation in upwelling winds is shown in Fig. 3. The convention of naming the transects according to the time (in hours) of observation relative to the beginning of our experiment is continued from PMK; 0 h refers to 0400 UTC 19 May. At +64 h, winds were upwelling favorable[4] and a significant alongshore current flowed southward 10–15 km offshore. Energetic turbulence was concentrated in a 5–10-m-thick BBL and occurred intermittently through the interior. At +85 h, decreasing southward winds preceded northward flow below 100-m depth at the offshore end of the transect, above which high ε was found. At this time, the BBL was still relatively thin. By +98 h, winds had further weakened and the BBL had thickened noticeably. After this time (+118 h), winds were northward and the BBL was at its thickest of the experiment (Fig. 4). By this point, mixed layer heights extended to 25 m above the bottom. The intense mixing in the BBL during the latter two of these transects is evident in the high values of ε across a wide range of the shelf (Fig. 3).

A series of consecutive individual profiles of potential temperature θ through the bottom boundary layer[5] from +118 h is shown in Fig. 5. These profiles cover a period of approximately 1 h and a cross-shore extent of 2 km. Although we have defined a mixed layer for each profile based on the location of a stably stratified layer above, it is clear that in detail these layers are not completely mixed. Within each profile are numerous examples of parcels of relatively warm (light) fluid beneath cool (dense) fluid. In the first profile of the sequence, a 6-m-thick layer of fluid adjacent to the bottom is 5 mK warmer than overlying fluid to a height of 20 m above the bottom. Other examples of relatively warm (light) fluid adjacent to the bottom are apparent throughout the sequence. Profiles of ε coincident with this sequence of θ profiles indicate large values near the bottom and considerable variability above (Fig. 5).

[3] Sensor tips are located 2 cm behind the protective ring. Insofar as the bottom is flat, measurements are made 2 cm from the bottom. Of course, the bottom is rough on many scales, and obstacles smaller than the ring diameter are occasionally captured within the ring, resulting in broken sensors—but only after completion of the profile 0 cm from the bottom. Because the bottom is rough over a range of scales, it also means that our estimate of height above the bottom is ill defined on scales of perhaps a few tens of centimeters or so.

[4] Wind stress, averaged over the 24-h period preceding each transect, is shown to the right on Fig. 3.

[5] Because our temperature measurement has better resolution (in relative terms) than our conductivity measurement, we show here potential temperature rather than potential density. We later show in averaged profiles that the superadiabatic potential temperature profiles are statically unstable.

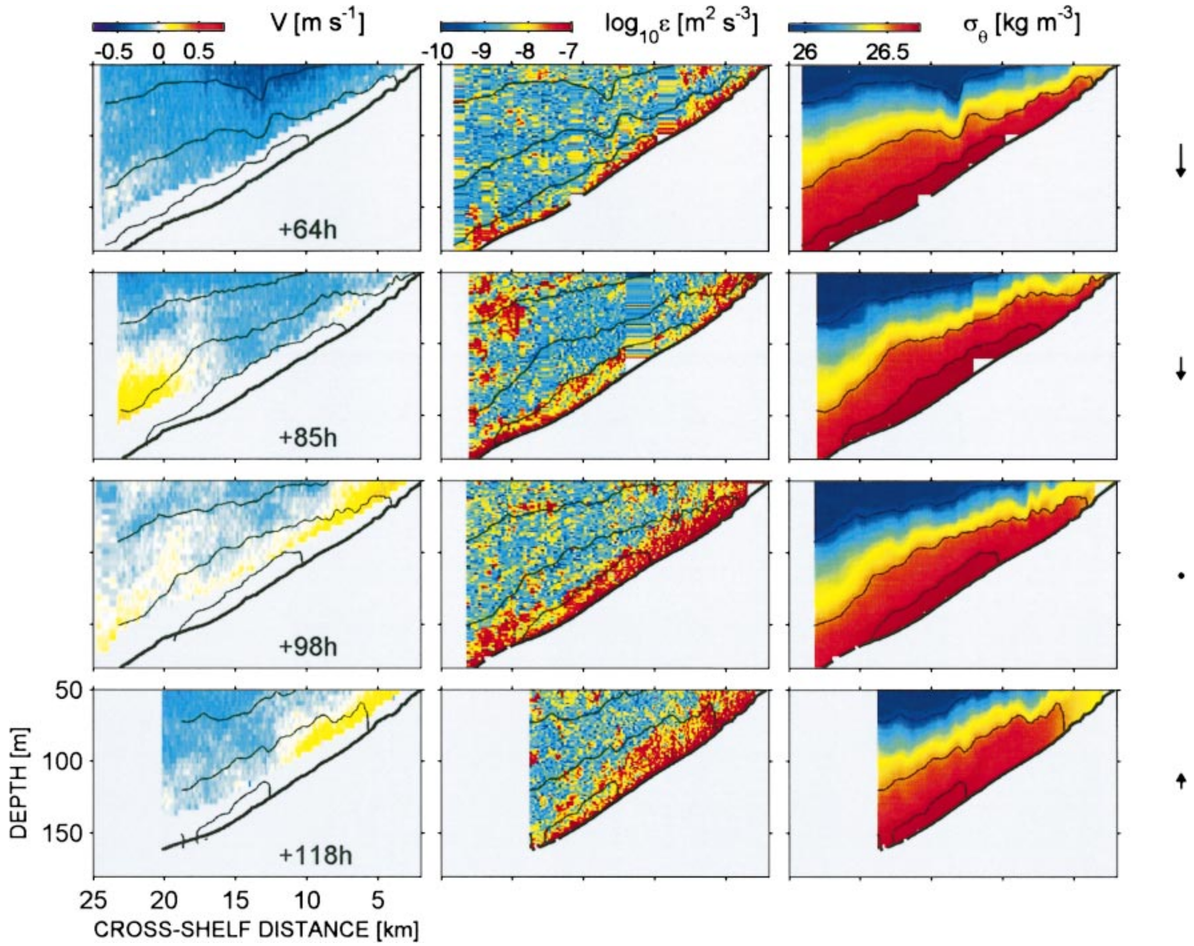

FIG. 3. Cross-shelf image plots of alongshore velocity V, turbulent kinetic energy dissipation rate ε, and potential density σ_θ at 45°02′N off Oregon. The cross-shelf distance is referenced to the 30-m depth contour at this latitude. Times shown in the V image plot are referenced to the first of 12 transects (0400 UTC 19 May) and indicate relative times between transects. The σ_θ contours of 26.0, 26.65, and 26.67 are plotted on each image plot. Arrows to the right indicate relative magnitude and direction of wind stress averaged over the 24 h prior to the transect; down is southward and upwelling favorable.

The first profile in the sequence suggests strong turbulence is restricted to the anomalously buoyant fluid at the bottom that has yet to be communicated to the mixed layer above.

The mean structure of the 17 profiles presented in Fig. 5 is shown in Fig. 6. Mean values of θ and σ_θ in the mixed layer, as determined from individual profiles, were first subtracted before averaging. These averaged profiles indicate three distinct regions. From the bottom up to about 11 m above the bottom, the gradient is superadiabatic (unstable). Here, $\partial_z\theta \simeq -1.7 \times 10^{-4}$ K m^{-1} and $\partial_z\sigma_\theta \simeq 6.0 \times 10^{-5}$ kg m^{-4} (mean gradients are shown as dashed lines in Fig. 6). From 11 to 14.5 m above the bottom, the mean profile indicates the stability is neutral—that is, $\partial_z\theta = \partial_z\sigma_\theta \simeq 0$. Above this, the mean profile is stable.

The mean profile of ε decreases with height from a maximum value of 6×10^{-7} m^2 s^{-3} at the bottom to a nearly constant value of 5×10^{-8} m^2 s^{-3} above 8 m. Also shown in Fig. 6 is the wall-layer scaling, $\varepsilon \simeq u_*^3/\kappa z$ (Tennekes and Lumley 1972). Height z is positive upward from 0 at the bottom, von Kármán's constant $\kappa = 0.4$, and friction velocity u_* was estimated by fitting the data in the lowest 5 m. The wall-layer scaling of ε is in approximate agreement with the observed mean profile over a greater range of z than is justified by either the range over which it was fit or by the height of the mixed layer D.

The example discussed here is not an isolated incident. In fact, the 2-km section shown in Figs. 5 and 6 represents the midpoint of a 6-km cross-shelf section of the BBL over which mean gradients in the lower 60% of the bottom mixed layer are unstable (Fig. 7). Cross-shelf gradients of θ and σ_θ determined relative to the sloping bottom are noted in Fig. 7. Cross-shelf gradients differ from horizontal gradients by $\cos\alpha$, where α is the bottom slope (Fig. 1). Here, $\alpha \sim 0.01$ and $\cos\alpha \simeq 1$.

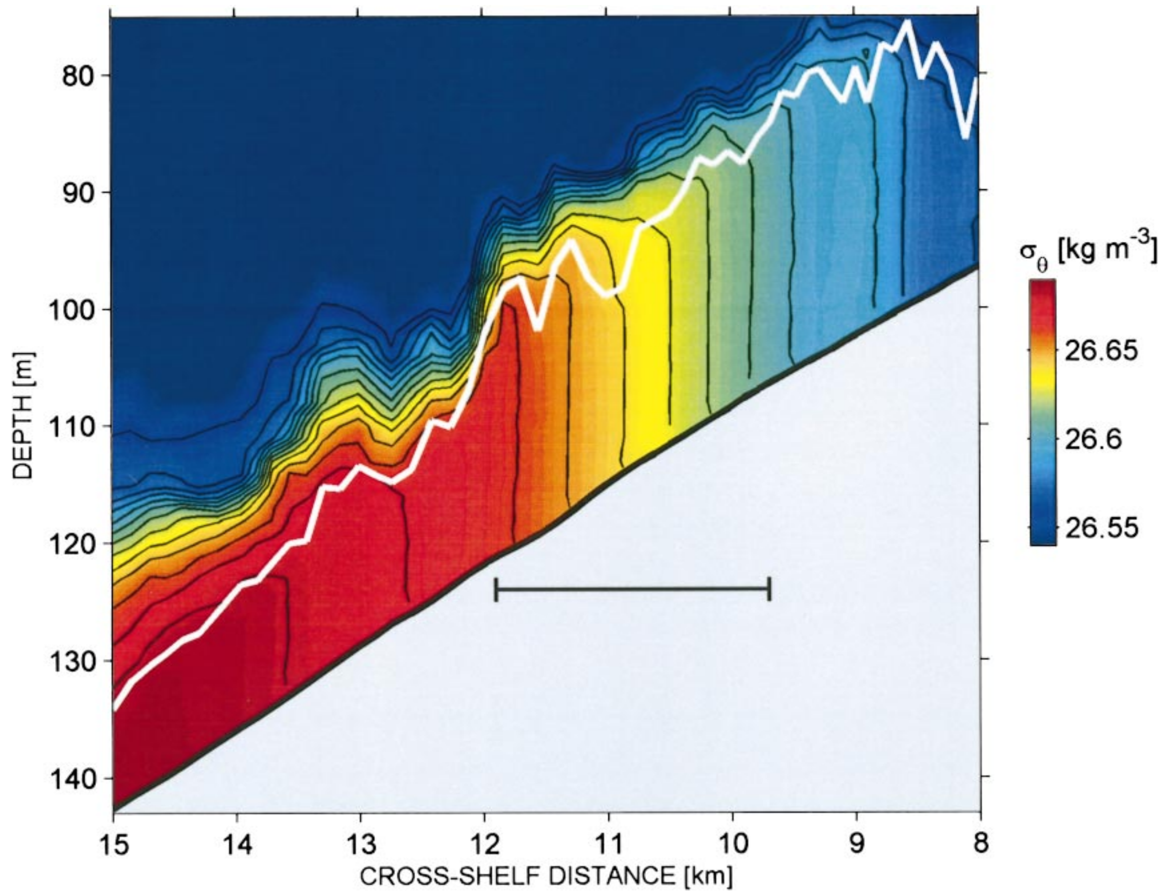

FIG. 4. Expanded plot of σ_θ in the BBL corresponding to +118 h in Fig. 3. The white line refers to the height of the mixed layer. The horizontal bar represents the region of the vertical profiles shown in Fig. 5.

3. Moored observations

The Coastal Ocean Advances in Shelf Transport[6] (COAST) north shelfbreak mooring (45°N, 124°12.7′W) located 1 km south of our transect line in 130-m water depth (location noted in Fig. 7) included temperature sensors 2 and 10 m above the bottom, a conductivity sensor at 10-m height and velocity profiles (300-kHz ADCP manufactured by RD Instruments, Inc.) above 12 m (Boyd et al. 2002).[7] A short record bounding the time of the observations discussed in the previous section is shown in Fig. 8. During this time, east–west currents were dominated by the semidiurnal tide. The semidiurnal tide was a significant feature of the north–south current variability, but there was also a change in direction of the currents in the lower 60 m from southward to northward in association with the weakening and reversal of winds from northerly to southerly. Following the reversal of the currents were several notable features in the near-bottom temperature structure. Beginning on 22 May with the current reversal, temperatures at 2 and 10 m above the bottom began to warm. This warming trend continued through the middle of 24 May at a mean rate of about 0.15 K day^{-1}, at which point bottom currents began again to reverse, this time to southward. As the warming progressed, the temperatures at 2 and 10 m became nearly equal, and toward the latter part of this period the temperature at 10 m was frequently cooler than that at 2 m, indicating static instability. The loss of high-frequency variability in the 10-m temperature record at this time indicates that the vertical extent of the mixed bottom fluid reached at least 10 m above the bottom.

The moored data clearly indicate a lag of about 1 day between the reversal of alongshore near bottom currents toward the north and the first appearance of an unstable temperature difference at the bottom. The near-bottom temperature structure is further modulated on a near-tidal period.

---

[6] The COAST program is funded by the National Science Foundation (NSF) Coastal Ocean Processes Program (CoOP).

[7] Because the temperature–salinity (T–S) relationship in the BBL was monotonic and well-defined at this time (PMK), we extrapolated the salinity at 10 m to 2 m to compute potential temperature at 2 m as well as at 10 m. The extrapolation agreed with our comparison of θ and S from Chameleon profiles.

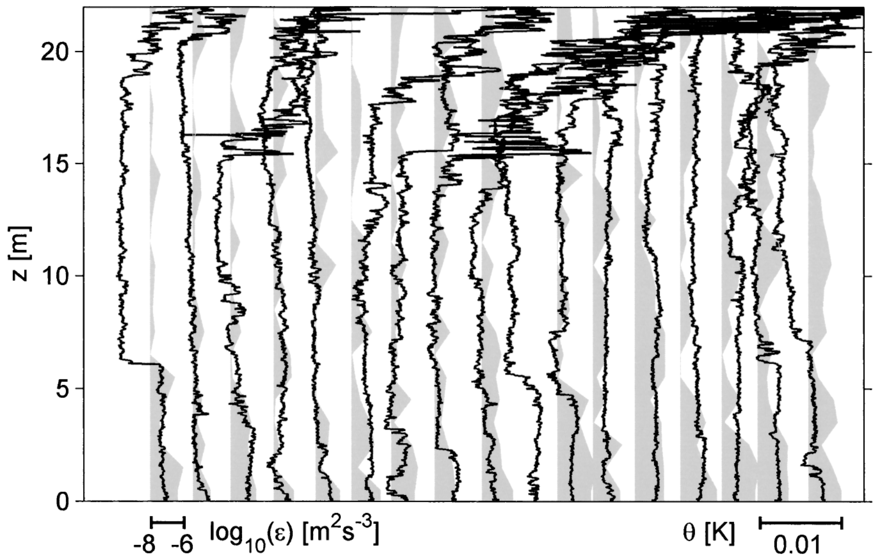

FIG. 5. Sequence of 17 vertical profiles of potential temperature (θ; black lines) and turbulence kinetic energy dissipation rate (ε; shaded gray) plotted vs height above the bottom z. Each θ profile was referenced to the potential temperature in the mixed layer by subtracting the averaged potential temperature in the mixed layer and is offset by 0.02 K from its neighbor. This sequence is from 10 to 12 km offshore during the +118-h transect shown in Figs. 3 and 4. The water depth ranges from 110 to 120 m (left to right in the direction of transit). Each profile is separated from the next by a little more than 3 min, or 120 m horizontally. Note that the tenth θ profile has no associated ε profile.

4. Mixed layer statistics

Statistics of mean values of mixed layer height D as well as density and potential temperature gradients for 2-km-averaged sections for the entire dataset of 12 cross-shelf transects are shown in Fig. 9. The mean value of D is 7.1 m, and the median is 6.8 m; the range is 1–22 m. The largest values were observed in transect +118 h, coinciding with the example shown in the previous section. These large values of D coincide with unstable BBLs, presumably associated with active convection. Vertical gradients of θ and σ_θ were computed between the bottom and 0.6D. The distributions of these are shown in the lower two panels of Fig. 9. Of the 141 2-km-averaged samples, the BBLs of 87 (62%) are stable ($\partial_z\sigma_\theta < -2 \times 10^{-5}$), 38 (27%) are neutral ($|\partial_z\sigma_\theta| < 2 \times 10^{-5}$), and 16 (11%) are unstable ($\partial_z\sigma_\theta > 2 \times 10^{-5}$). The 6-km stretch across the shelf from about 5 to 11 km in transect +118 h is clearly the largest contiguous unstable BBL observed (Fig. 7). We note that a few other examples of unstable BBLs were found intermittently throughout the other transects, including times at which upwelling circulation dominates. However, these events were typically of more limited lateral extent.

Statistics of the unstable mixed layers are shown in Fig. 10. For each of the mixed layers identified as unstable in a 2-km average, the mean thickness (δ_{ul}) of the unstable part of the profile was determined. The mean value of the ratio δ_{ul}/D is ≈ 0.5. We note that the mean value of D for this subset of the data is greater than the experiment mean. This result is due to the much thicker mixed layers found during the periods of convectively driven mixing.

For each 2-km section over which the bottom boundary layer was unstable, the maximum density anomaly ($\delta\rho_{max}$) in the individual profiles was determined over height δ_{ul} and was compared with ε_{ml}, the mean value of ε in the neutral layer (the mean was computed over the interval $\delta_{ul} < z < D$; Fig. 11). Higher values of ε_{ml} are clearly associated with higher values of $\delta\rho_{max}$.

5. Rayleigh number

The process of convection is associated with the generation of localized plumes of rising light fluid or sinking dense fluid. The motion of plumes is retarded by viscous forces, and the buoyancy is dissipated by thermal diffusion as the plumes rise into fluid of lower temperature. If the buoyancy force is too weak to overcome viscous inhibition plus thermal diffusion, a statically unstable density profile may persist in the absence of convection. The relative importances of viscosity, diffusion, and buoyancy are related by a Rayleigh number (Turner 1973)

$$\mathrm{Ra} = \frac{g\rho' d^3}{\rho K_T \nu}, \tag{1}$$

where $g = 9.8$ m s^{-2} is the gravitational acceleration, $K_T = 1.4 \times 10^{-7}$ m^2 s^{-1} is the thermal diffusivity in seawater, $\nu = 1 \times 10^{-6}$ m^2 s^{-1} is the kinematic viscosity,

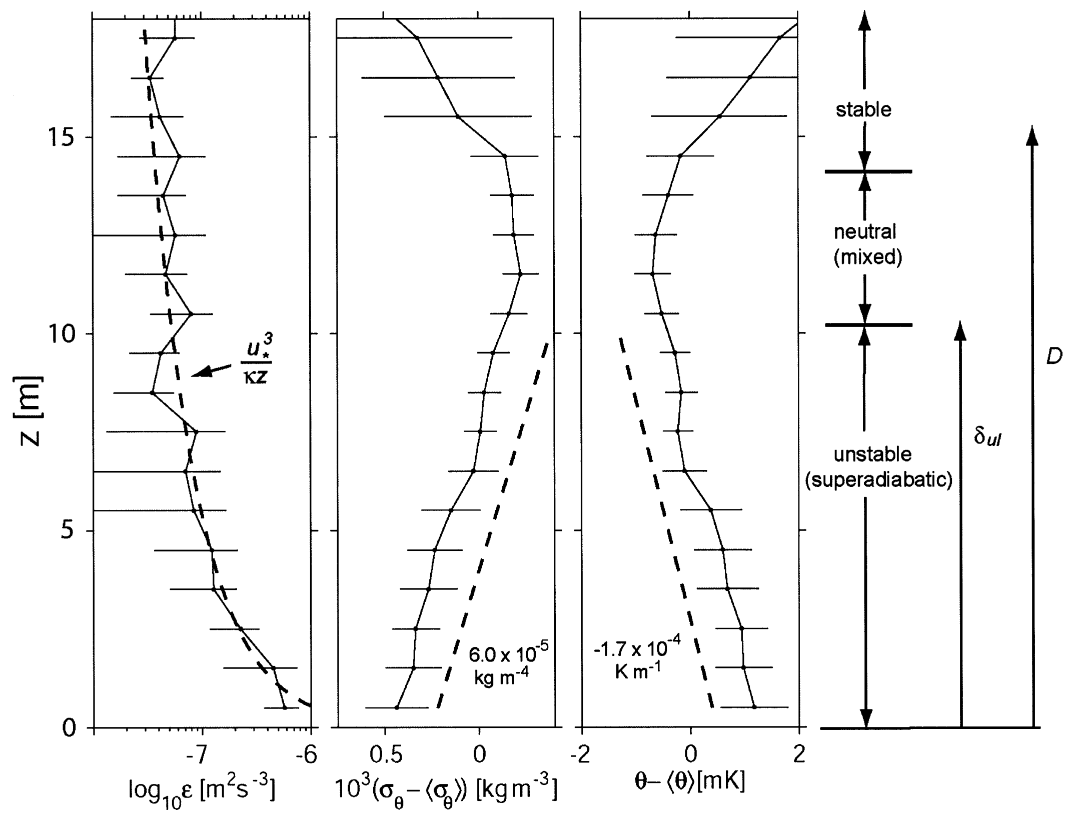

FIG. 6. Profiles of ε, σ_θ, and θ averaged over the profiles shown in Fig. 5. For σ_θ and θ, the mean value in the mixed layer was first subtracted before averaging. The dashed line in the ε profile represents the wall-layer scaling $u_*^3/(\kappa z)$ with $u_* = 0.006$ m s^{-1}. The dashed lines in the profiles of σ_θ and θ indicate the mean gradients. Also indicated to the right are δ_{ul} and D.

d is the thickness of the convective layer, ρ is density, and ρ' is the density anomaly.

Convection occurs when the buoyancy anomaly (or Ra) is sufficiently large. In the case of fluid bounded above and below by rigid plates, the critical value of Ra is $O(10^3)$ (Turner 1973). Our observations indicate $d \sim 20$ m and $\rho'/\rho \sim 10^{-6}$, corresponding to the 0.005-K temperature anomaly in Fig. 5. These values give Ra $\sim 10^{11}$.

6. Analogy to upper-ocean convection

The individual profiles shown in Fig. 5 bear a strong resemblance to those obtained in the mixed layer of the upper ocean during convection (Fig. 1 from Anis and Moum 1992). The magnitude of the temperature (buoyancy) anomalies are the same but are of opposite sign. Variability of the vertical scales and the magnitudes of the anomalies are similar both within the mixed layer and from profile to profile.

Further comparison with upper-ocean convection, from an experiment in which surface forcing was documented well, comes from the study by Anis and Moum (1994). The data from night 3 were plotted by Anis and Moum (1994) as nondimensional depth (z/D) versus nondimensional dissipation (ε/J_b^0, where J_b^0 is the surface buoyancy flux determined from surface meteorological measurements).[8] In Fig. 12 we plot these data as dimensional dissipation versus nondimensional depth (light gray). For comparison with the BBL profiles, upper-ocean depth and θ scales are inverted. For comparison with the upper-ocean data, individual BBL profiles were first nondimensionalized by D before averaging. Profiles of $\theta(z/D)$ and $\varepsilon(z/D)$ are shown in dark gray in Fig. 12. Both upper-ocean and BBL observations were made from the stern of a ship using a loosely tethered profiler. Although BBL observations include data to within 2 cm of the bottom, profiling in a ship wake limits the proximity to the sea surface at which useful data can be obtained.

The upper-ocean data exhibit four distinguishing characteristics, which appear to be general to convectively mixed layers in ocean and atmosphere and are demonstrated in Fig. 12. First, the θ profile is superadiabatic (alternatively, the σ_θ profile is statically unstable) in a region extending from very near the surface to approximately 0.4D. In the case of the upper ocean,

[8] The data from night 3 are typical and representative. They also are the data shown by Anis and Moum (1992).

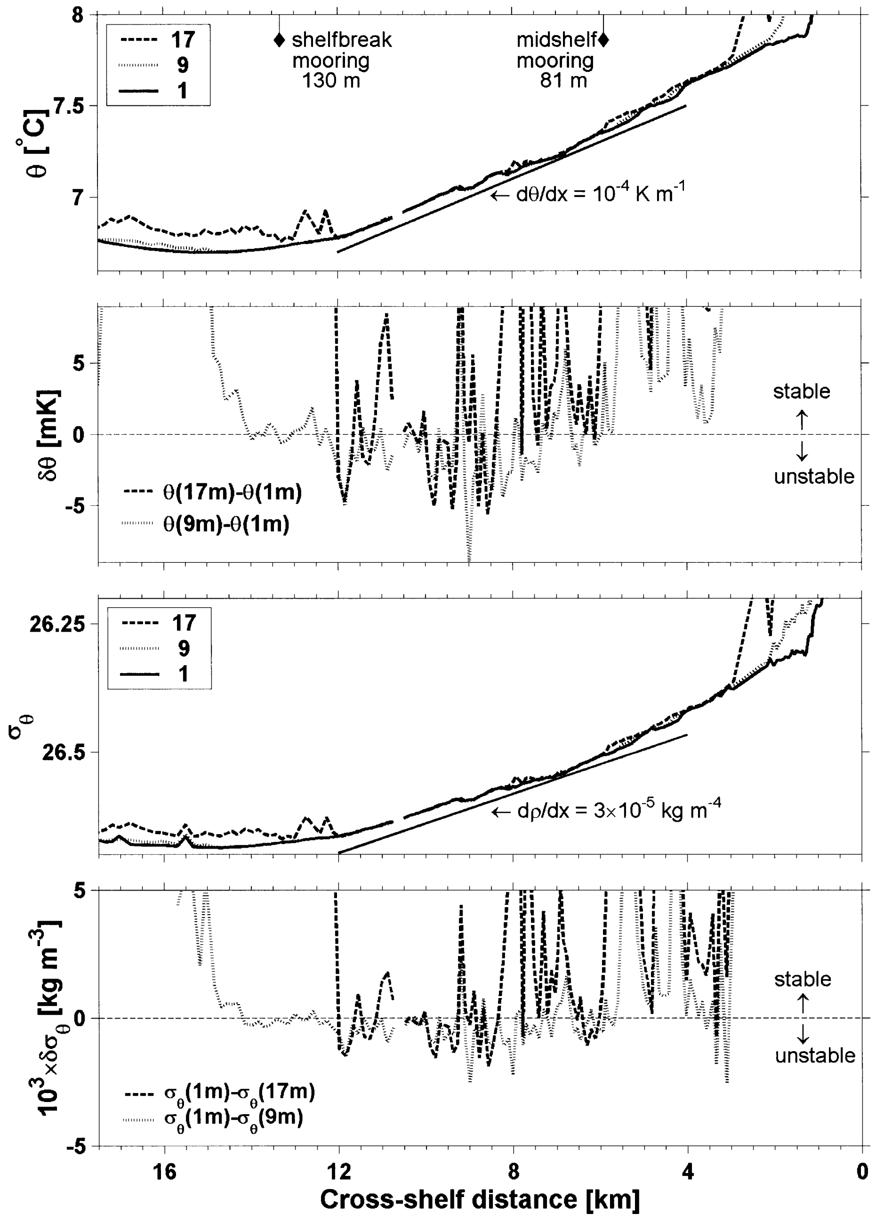

FIG. 7. Cross-shelf distribution of temperature and density in the BBL. (top) Temperature 1, 9, and 17 m above the bottom as determined from 178 vertical Chameleon profiles. The mean value of the cross-shelf temperature gradient of 10^{-4} K m^{-1} is noted. (second from top) The difference in temperature between bottommost bin (1 m) and 9 and 17 m above the bottom. The convention of differencing is such that negative values are unstable. (third from top) Density; the mean value of the cross-shelf density gradient is 3×10^{-5} kg m^{-4}. (bottom) The difference in density between bottommost bin (1 m) and 9 and 17 m above the bottom. Negative values of the density differences are statically unstable.

surface cooling creates the structure of relatively cool fluid atop warm fluid. In the atmospheric boundary layer, relatively warm fluid lies beneath cooler fluid when the air near the surface is heated from below through a viscous microlayer. The second distinguishing feature is that beyond this superadiabatic surface layer (downward from the ocean surface, upward from the atmosphere's surface) there is a neutral layer defined by $\partial_z \theta = 0$. A third feature is the increase of ε toward the surface in the unstable layer. In the case of nonzero wind stress over land, the shape of $\varepsilon(z)$ in the surface layer is approximated by surface-layer scaling. In the upper ocean, the influence of breaking surface gravity waves and Langmuir circulations cause an increase of $\varepsilon(z)$ toward the surface that is greatly increased over wall-layer scaling (Anis and Moum 1995; Terray et al. 1996). The

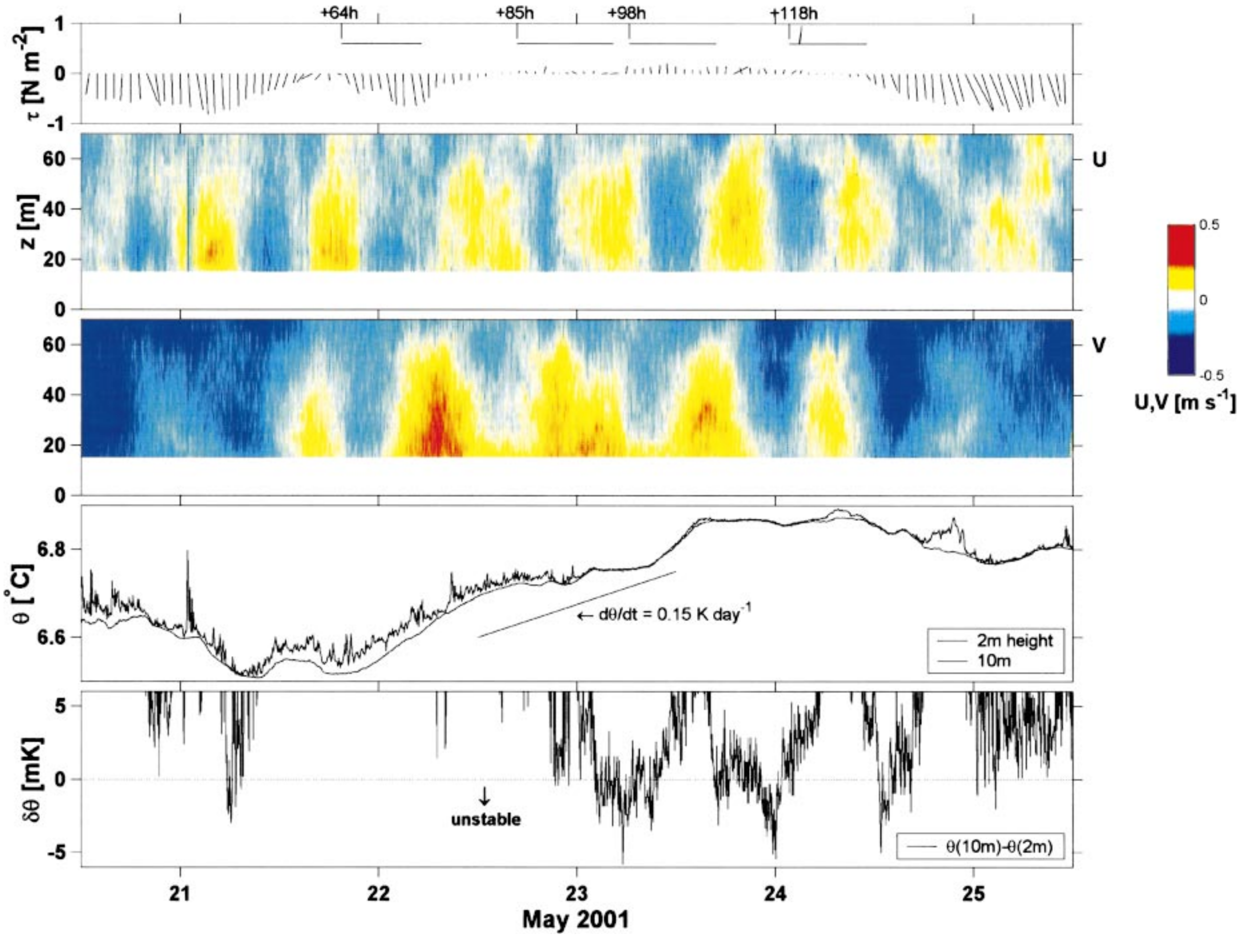

FIG. 8. Time series of (top) wind stress from the COAST meteorological buoy at 44°59.8′N, 124°7.0′W), (second from top) cross-shelf velocity, (middle) alongshore velocity, (second from bottom) potential temperature at 2 and 10 m above the bottom, and (bottom) the difference between the two potential temperature series shown. The temperature difference is unstable when negative. The horizontal lines in the top panel represent the times of transects shown in Fig. 3. The slope of the line in the fourth panel is denoted as 0.15 K day^{-1}.

fourth feature is that, away from the surface layer but within $z/D < 1$, ε is nearly constant with depth and is equal to the buoyancy flux at the surface (at the sea surface, this is denoted J_b^0). In detail, $\varepsilon(z)$ varies linearly with depth, a requirement of a linear buoyancy flux profile through the mixed layer when the dominant forcing is buoyancy (Anis and Moum 1994).

Each of the four general distinguishing features of θ and ε profiles in convectively mixed layers is apparent in the averaged BBL profiles (Fig. 12). The superadiabatic surface layer extends to about 0.4D, below which ε increases toward the bottom. Above 0.4D, both θ and ε are nearly constant with height. The magnitude of θ_z, -1.7×10^{-4} K m^{-1}, is nearly equal to that from the upper-ocean data shown here. Although the gradients are the same, the net difference in θ over the surface layer differs in accordance with the differences in D (BBL data indicate $D \approx 20$ m; $D \approx 50$ m for the upper-ocean data).

Near the seafloor, the turbulence is predominantly stress driven, which accounts for the increase in ε toward the bottom. Numerous analyses have shown the turbulence here to agree reasonably with wall-layer scaling (Dewey and Crawford 1988; Nash and Moum 2001; Perlin et al. 2004a, manuscript submitted to *J. Geophys. Res.*, hereinafter PMKLBK) permitting an estimate of the bottom stress ($\tau_b = \rho u_*^2$), where u_* is determined from the dissipation profile. The Monin–Obukhov length scale L_{MO} [$=u_*^3/(\kappa J_b)$] relates the relative contribution of bottom stress-driven turbulence and buoyancy flux to the turbulence in the BBL ($\kappa = 0.4$ is von Kármán's constant); L_{MO} represents the depth at which buoyant production of turbulence kinetic energy (TKE) and stress-driven production of TKE are equivalent. If $D \gg L_{\mathrm{MO}}$, then there ought to be a depth range for which the turbulence is dominated by convection.

If the averaged profile of ε from the BBL shown in Fig. 12 is a consequence of convectively driven mixing, then, just as in the upper ocean or the lower atmosphere during convection, the buoyancy flux forcing the turbulence should be equal to $\varepsilon_{\mathrm{ml}}$. We denote this flux as J_b^H, where H refers to the ocean bottom. From Fig. 12,

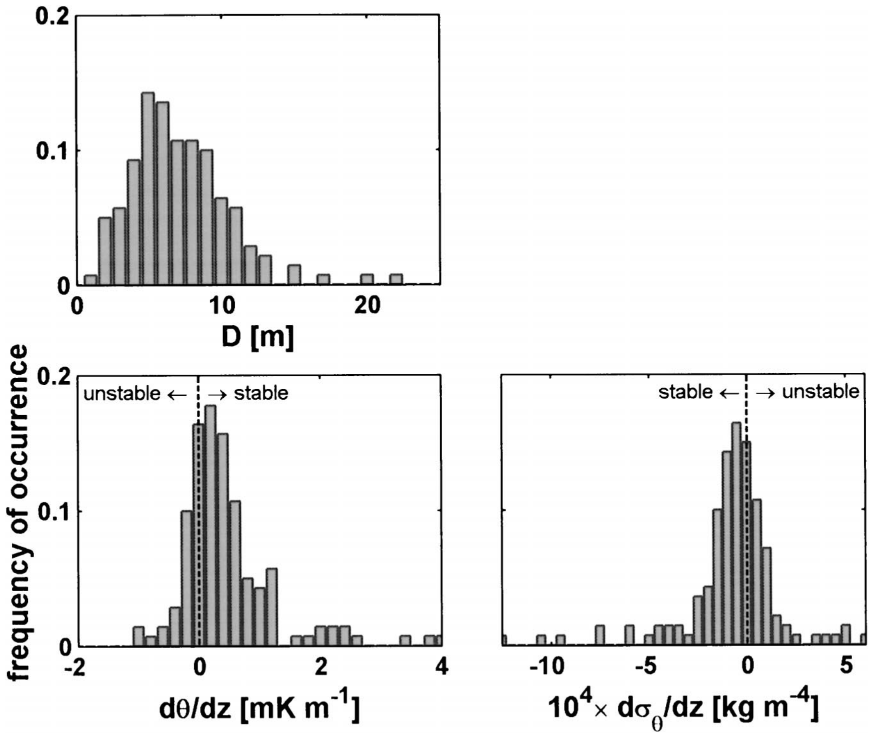

FIG. 9. Bottom mixed layer statistics over the entire 8-day, 12-transect experiment, based on 2-km cross-shore averages. (top) The distribution of mixed layer heights D. (lower left) The distribution of temperature gradients in the mixed layer, and (lower right) the distribution of density gradients. For this calculation, the gradients were computed from the surface to 0.6D. The total number of samples is 141. Of these, 87 (62%) are stable ($\partial_z\sigma_\theta < -2 \times 10^{-5}$), 38 (27%) are neutral ($|\partial_z\sigma_\theta| < 2 \times 10^{-5}$), and 16 (11%) are unstable ($\partial_z\sigma_\theta > 2 \times 10^{-5}$).

$J_b^H \approx 6 \times 10^{-8}$ m^2 s^{-3}. The value of the Monin–Obukhov length scale relevant for the bottom mixed layer [$L_{\mathrm{MO}}^H = u_*^3/(\kappa J_b^H)$] is shown in Fig. 12 to be about 0.25D (in dimensional terms, 5 m), which is close to that for the upper-ocean example depicted. In turn, this suggests that a depth range exists over which we might expect buoyancy forcing to dominate the generation of TKE.

Other than the small geothermal heat flux, the buoyancy flux (J_b^H) at the bottom must be 0. In this sense, the analogy with convection in the upper ocean and lower atmosphere is not correct. In Fig. 1, we have indicated J_b^H acting at height δ_{ul}. Although this is also incorrect, it suggests that the observed superadiabatic profiles are a result of the advection of buoyant fluid beneath denser fluid. The Ekman-induced advection of buoyant fluid down the slope is discussed in the next section.

7. Cross-shelf buoyancy source

The source of buoyancy in the BBL responsible for driving convection must be the cross-shelf density gradient that results from the upslope Ekman transport of dense fluid during upwelling. Subsequent downwelling results in an offshore transport of light fluid in the BBL beneath denser fluid above. As a consequence, the vertical gradient of buoyancy is produced by lateral advection. PMK have established that offshore movement of the locations of isopycnal intersections with the bottom occurs during downwelling and that their speed is in agreement with the prediction from Ekman dynamics using the bottom stress estimated from our observations. Typical offshore velocities[9] during downwelling were estimated by PMK to be 1–4 km day^{-1}.

Such small cross-shelf velocities are obscured in moored observations by much larger and higher-frequency tidal velocities. A representative current speed profile [$V(z)$] that follows the modified law of the wall proposed by PMKLBK is shown in Fig. 13. From moored observations, Perlin et al. (2004, manuscript submitted to *J. Geophys. Res.*) determined an Ekman veering angle [$\Theta(z)$] in the BBL similar to that in Fig. 13 [here, $\Theta(z) = 0$ due north and increases clockwise]. Together, these give a cross-axis velocity [$V(z)\sin\Theta(z)$] profile as shown in Fig. 13. In the case that $V(z)$ is northward, the cross-axis velocity is offshore. The result is a concentration of Ekman transport in the lower 5 m.

[9] These estimates were made from both the observed cross-shelf displacement of isopycnal intersections with the bottom and a dynamic estimate of bottom Ekman transport from local bottom stress estimates (using our turbulence profiles).

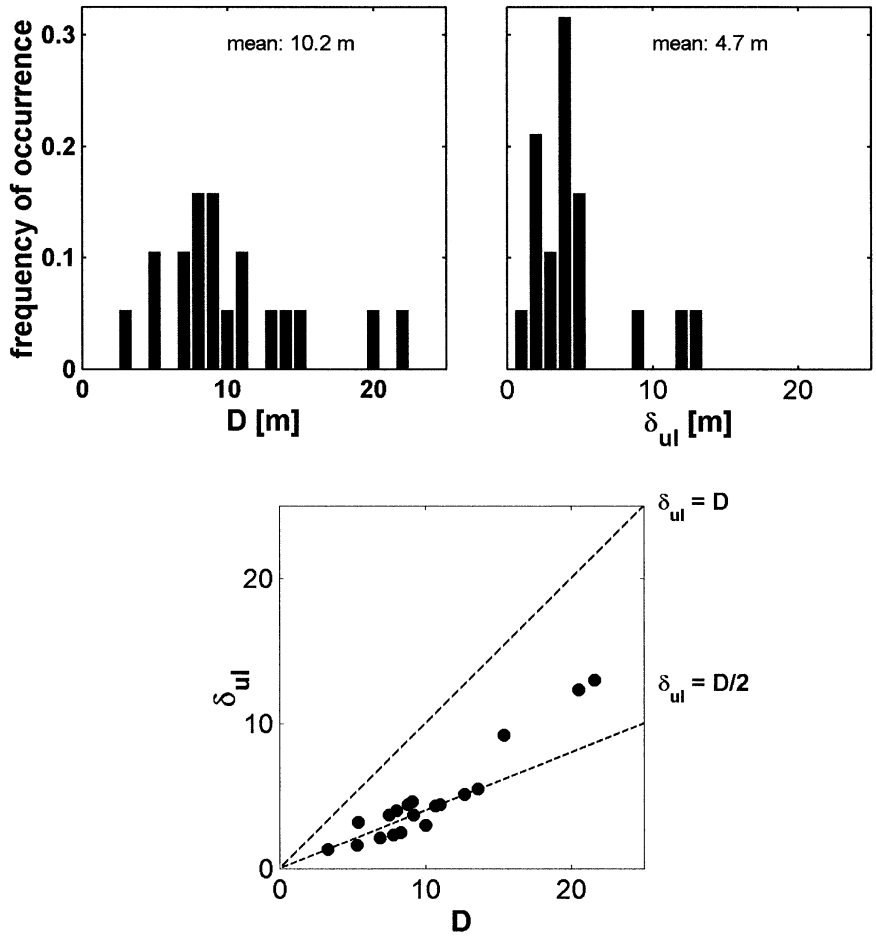

FIG. 10. Distributions of (top left) mixed layer height D and (top right) unstable layer (δ_{ul}) thicknesses for those 2-km-averaged sections with unstable mixed layers shown in Fig. 9. (bottom) A plot of D vs δ_{ul}.

The difference in velocity between 3-m height and the top of the Ekman layer is 0.015 m s^{-1} ($\sim$1.5 km day^{-1}). We suggest the possibility that this provides the differential transport of buoyant bottom fluid necessary to generate convective instability in the bottom boundary layer.

To construct a scaling argument, we suppose that J_b^H is balanced by offshore advection of buoyancy,

$$J_b^H = \frac{g}{\rho}\int_0^h u\frac{\partial \rho}{\partial x}\,dz, \tag{2}$$

where $z = 0$ at the bottom and increases upward, h represents the thickness of the layer within which the buoyancy is trapped, and $\partial\rho/\partial x$ is the local cross-shore density gradient (shown in Fig. 7). In the case in which u and $\partial\rho/\partial x$ are depth independent,

$$J_b^H = \frac{gh}{\rho}u\frac{\partial \rho}{\partial x}. \tag{3}$$

A reasonable choice for h is suggested from an examination of Fig. 5. The first profile in this sequence shows a 6-m-thick bottom layer of fluid with positive buoyancy anomaly. Within the layer the turbulence is active; above it is small. One possibility is that the buoyancy anomaly has yet to be communicated via convection to the full extent of the mixed layer. This may be an example of the early stages of formation of a buoyant plume. Subsequent profiles indicate a general trend toward increasing turbulence in the mixed layer; the final profiles in the sequence suggest a fairly uniform distribution of turbulence throughout the mixed layer to a height of 20 m above the bottom. Here, we might consider the buoyancy anomaly associated with the 5-mK temperature anomaly in the first profile distributed over the 5-m depth to represent the advective source in Eq. (3). In this case, the mean value of $\partial\rho/\partial x = 3 \times 10^{-5}$ kg m^{-4} (from Fig. 7) leads to an estimate for the advective velocity u of approximately 2 km day^{-1}.

This scale estimate for u is comparable to the local estimate of the bottom Ekman velocity (PMK) and is consistent with the cross-axis velocity in the lower 5 m shown in Fig. 13. This estimate is also consistent with

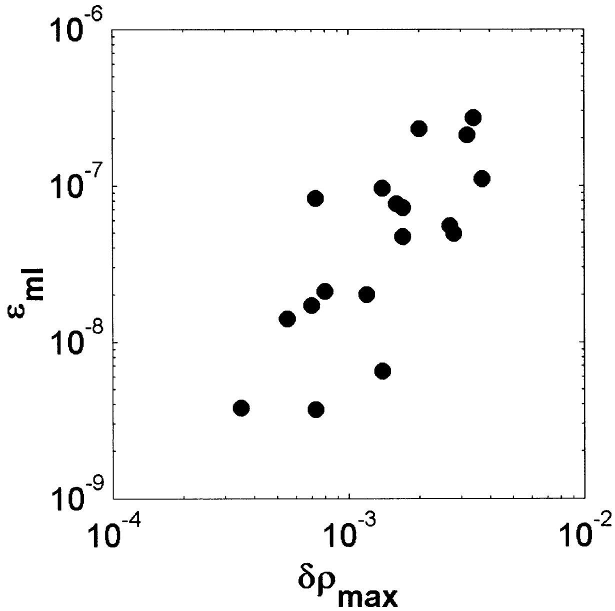

FIG. 11. Plot of maximum density anomaly $\delta\rho_{max}$ vs ε_{ml}, the mean value of ε in the neutral layer from 2-km-averaged data.

the time rate of change of potential temperature observed near the bottom from the mooring at 130-m water depth near the location of our detailed profiler observations of convection. That is, we have inferred the local fluid warming, $\partial_t\theta$, from moored observations to be $\simeq$0.15 K day^{-1} (Fig. 8). In the case that this is due to offshore lateral advection, $u\partial_x\theta \sim 0.2$ K day^{-1}, where $u \sim 2$ km day^{-1} and $\partial_x\theta \sim 10^{-4}$ K m^{-1} (from Fig. 7). So, our velocity scale estimate, combined with observed cross-shelf temperature structure, is consistent with the independently observed heating rate.

A characteristic time scale for the turbulence in the BBL during convection comes from similarity scaling (e.g., Shay and Gregg 1986). This represents the time scale for convective overturns and is given by

$$T \sim \left(\frac{D^2}{J_b^H}\right)^{1/3}, \tag{4}$$

where the characteristic length scale is taken to be the mixed layer height D. In the example we have presented here, $T \approx 2000$ s. Moored observations indicate that periods of static instability last for many hours (Fig. 8). Cross-shelf transects indicate that, during these periods of static instability, large regions of the bottom (several kilometers) are affected. These events are local neither in space nor in time. Durations of events are many times T and lateral scales are many times D.

Associated with T is an overturning velocity scale, $w \sim D/T \simeq 0.01$ m s^{-1}. This value is comparable to both the scale estimate derived from a cross-shelf buoyancy source and to the cross-axis velocity estimated from the observed profiles of velocity and veering angle in the BBL. It suggests that the cross-shelf supply of buoyancy is sufficient to maintain convectively driven overturning in the BBL.

8. Discussion and summary

Convection in the BBL is inferred from the following observations.

1) Vertical profiles of θ and σ_θ indicate a superadiabatic layer near the bottom.
2) The large value of Ra suggests the presence of sufficient buoyancy to overcome the retarding effects of viscosity and thermal diffusion in generating buoyant plumes.
3) Higher values of buoyancy anomaly are associated with higher values of ε within the neutral layer.
4) The vertical structures of averaged profiles of σ_θ, θ, and ε are similar to their distinctive structure in the mixed layer of the upper ocean during convection.
5) The cross-shelf, Ekman-induced supply of buoyant fluid near the bottom is sufficient to support the inferred buoyancy flux.
6) Moored records indicate that periods over which the BBL is statically unstable are many times T, and cross-shelf transects indicate that regions of the shelf that are statically unstable during these periods are many times D. Together, these suggest that convective overturns have sufficient time to develop and to mix the BBL.

In this analysis we have presented some details of one episode during which near-bottom temperature differences were mixed and unstable from the perspective of a nearly coincident mooring. The moored data indicate a sequence that begins with the reversal of surface winds from upwelling- to downwelling-favorable. This is followed by a reversal of currents in the bottom 60 m (not to the surface) from southward to northward, an increase in temperature near the bottom, an increase in the depth of the bottom mixed layer from less than 10 to greater than 10 m and frequent occurrences of static instability in which the potential temperature at 10 m was lower than that at 2 m.

The moored record indicates that events such as we have shown here, although not identical, are the rule following surface wind reversals. This is seen in the records at both mooring locations indicated in Fig. 7. At the midshelf mooring location, a temperature sensor at 24 m indicated that the bottom layer frequently mixed to heights greater than 24 m during bottom convection. Over the 3-month duration of the mooring deployments, each mooring witnessed 10 events of northward near-bottom flow lasting at least one day (although modulated on tidal periods as is the event shown in Fig. 8). At the midshelf location (80-m water depth), the seven most intense of these coincided with $\delta T < 0$. At the shelfbreak location (130-m water depth), the eight most intense events of northward near-bottom flow coincided with $\delta T < 0$.

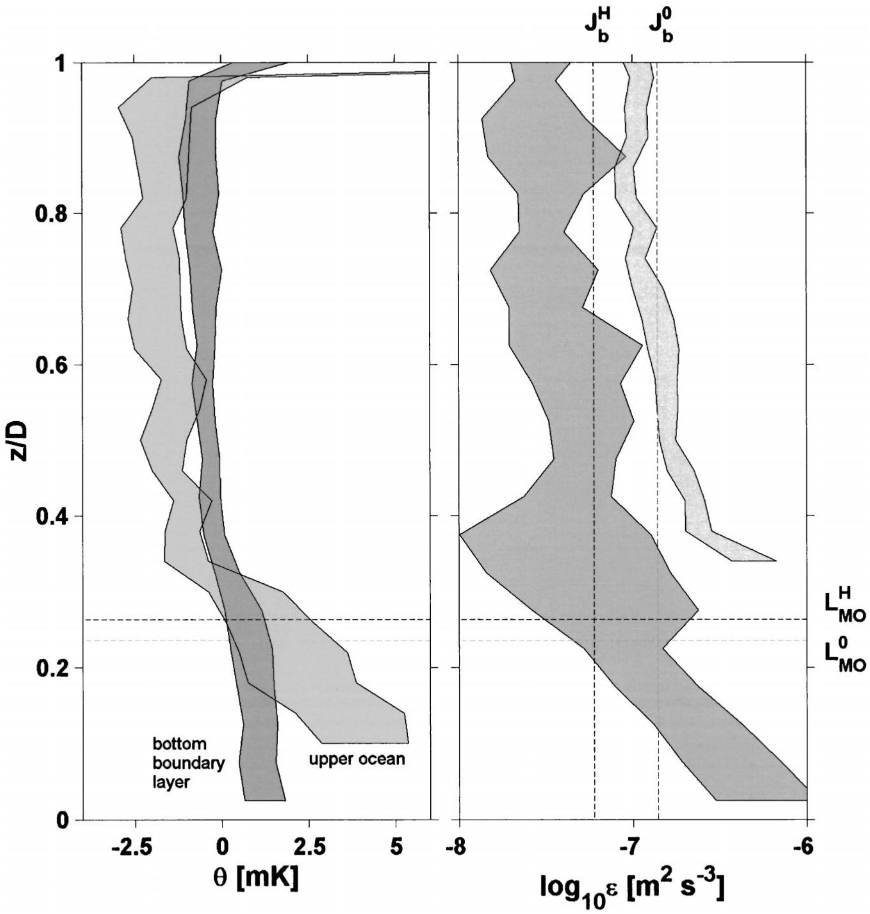

FIG. 12. Profiles of ε and θ plotted vs nondimensional depth z/D (dark gray). Individual profiles were nondimensionalized by their mixed layer height, and mean values of mixed layer temperature were removed prior to averaging. For comparison, data from the upper ocean during convection are plotted with z/D and θ axes inverted (light gray). The upper-ocean data are derived from night 3 of Anis and Moum (1994). Surface buoyancy flux J_b^0 and Monin–Obukhov length scale L_{MO}^0 were determined from surface meteorological data (Table 1 of Anis and Moum 1994). Bottom buoyancy flux J_b^H was estimated as the mean value of ε in the mixed layer, and bottom M-O length scale (L_{MO}^H) was estimated from J_b^H and u_* determined by fitting the near-bottom ε profile shown in Fig. 6. Mean values of D are 20 m for the BBL data and 50 m for the upper-ocean data.

This sequence of events is consistent with the offshore Ekman flow in the BBL that must result from a northward flow above. The local fluid warming observed at the mooring is due to offshore Ekman transport of lighter fluid from up the slope. Static instability follows as differential advection within the bottom layer moves light fluid beneath denser fluid. This can occur as a result of the concentration of cross-axis Ekman transport in the lower part of the Ekman layer, as suggested from the profiles shown in Fig. 13. The resultant structure of density in the BBL is indicated in Fig. 1 and is intended to represent the influence of the inferred velocity profile in the absence of mixing. The convectively driven mixing that must inevitably follow will alter this structure to be nearly mixed. The remnant of this inferred structure is the observed superadiabatic density profile near the bottom.

The time lag between the turning of near-bottom currents to the north and the appearance of an unstable temperature difference at the bottom (Fig. 8) must be due to at least two factors. First of all is the time required to spin up a bottom Ekman layer with an offshore flow component. Second, fluid must be drawn down the slope some distance in order for isopycnals to steepen (eventually becoming vertical and thence unstable). The time required for steepening must depend on both the cross-shelf velocity near the bottom and the cross-shelf stratification in the bottom boundary layer.

The mechanism we have proposed to create the conditions for instability in the BBL is independent of the tides. However, there is a tidal signal in the velocity (both cross shelf and along shelf) and there does appear to be a tidal modulation of the unstable temperature differences near the bottom in the moored record shown

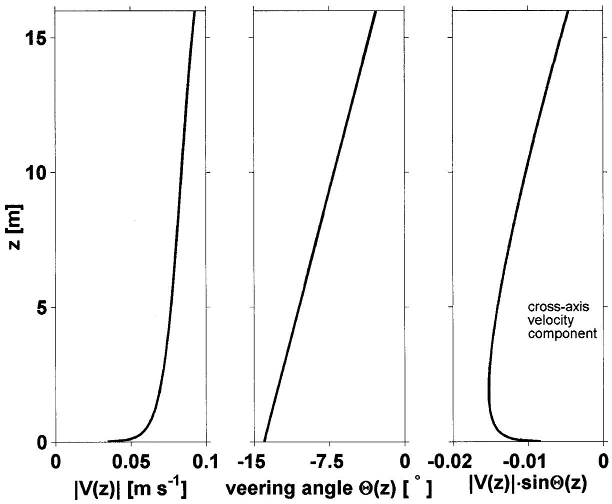

FIG. 13. Representative profile of horizontal velocity in the BBL following a modified logarithmic velocity profile proposed by PMKLBK. (middle) Veering angle of the current toward the bottom as indicated from 0.5-m-resolution acoustic velocity profiler (2-MHz ''Aquadopp'' manufactured by Nortek AS) on the north midshelf mooring (45°N, 124°7.0′W). (right) Cross-axis velocity component determined from the vertical profile of the product of the velocity and the sine of the veering angle. In the case that the velocity $V(z)$ is northward alongshore, the cross-axis velocity is offshore everywhere above the bottom.

in Fig. 8. Three possibilities arise. It is possible that tidal maxima in the northward velocity lead to increased offshore Ekman flow, creating buoyant instabilities locally. However, this requires an Ekman response on a time scale significantly shorter than an inertial period and hence seems unlikely. An alternative is that fluid is simply advected across the shelf by the cross-shore component of tidal velocity, and unstable fluid appears and disappears from the mooring's field of view on a tidal period. It is also possible that tidal current shear at times of onshore flow (because velocity must = 0 at the bottom) can enhance the vertical buoyancy anomaly; offshore tidal flow will diminish the buoyancy anomaly. Further analysis and modeling are required to understand the relative influences of Ekman flow and tides in this process.

The scenario we have suggested is two-dimensional. Yet the larger component of the flow above the bottom is alongshore, not cross-shore, because veering angles are much less than 45° (Fig. 13). Our scenario requires that the alongshore variability in the BBL is much less than the cross-shore variability, an issue that will require observation beyond the scope of this experiment.

Acknowledgments. This work was funded by the NSF as part of the CoOP program Coastal Ocean Advances in Shelf Transport. We acknowledge the assistance of Mike Neeley-Brown, Ray Kreth, and Greig Thompson, and the constructive comments of two anonymous reviewers. Greg Avicola made helpful comments on an early draft of the manuscript. We also thank Walt Waldorf, Dennis Root, and Steve Gard for their assistance in the mooring project.

REFERENCES

Anis, A., and J. N. Moum, 1992: The superadiabatic surface layer of the ocean during convection. *J. Phys. Oceanogr.,* **22,** 1221–1227.

——, and ——, 1994: Prescriptions for heat flux and entrainment rate in the upper ocean during convection. *J. Phys. Oceanogr.,* **24,** 2142–2155.

——, and ——, 1995: Surface wave–turbulence interactions: Scaling $\varepsilon(z)$ near the sea surface. *J. Phys. Oceanogr.,* **25,** 2025–2045.

Boyd, T., M. D. Levine, P. M. Kosro, S. R. Gard, and W. Waldorf, 2002: Observations from moorings on the Oregon continental shelf, May–August 2001: A component of the Coastal Ocean Advances in Shelf Transport (COAST) experiment. COAS Data Rep. 190 2002-6, Oregon State University, 195 pp.

Brubaker, J. M., 1987: Similarity structure in the convective boundary layer of a lake. *Nature,* **330,** 742–745.

Caughey, S. J., and S. G. Palmer, 1979: Some aspects of turbulence structure through the depth of the convective boundary layer. *Quart. J. Roy. Meteor. Soc.,* **105,** 811–827.

Dewey, R. K., and W. R. Crawford, 1988: Bottom stress estimates from vertical dissipation rate profiles on the continental shelf. *J. Phys. Oceanogr.,* **18,** 1167–1177.

Hosegood, P., and H. van Haren, 2003: Ekman-induced turbulence over the continental slope in the Faeroe–Shetland Channel as inferred from spikes in current meter observations. *Deep-Sea Res.,* **50,** 657–680.

Imberger, J., 1985: The diurnal mixed layer. *Limnol. Oceanogr.,* **30,** 737–770.

Lentz, S. J., and J. H. Trowbridge, 1991: The bottom boundary layer over the continental shelf. *J. Phys. Oceanogr.,* **21,** 1186–1201.

Lombardo, C. P., and M. C. Gregg, 1989: Similarity scaling of viscous and thermal dissipation in a convecting surface boundary layer. *J. Geophys. Res.,* **94,** 6273–6284.

MacCready, P., and P. B. Rhines, 1993: Slippery bottom boundary layers on a slope. *J. Phys. Oceanogr.,* **23,** 5–22.

Moum, J. N., M. C. Gregg, R. C. Lien, and M. E. Carr, 1995: Comparison of turbulence kinetic energy dissipation rate estimates from two ocean microstructure profilers. *J. Atmos. Oceanic Technol.,* **12,** 346–366.

Nash, J. D., and J. N. Moum, 2001: Internal hydraulic flows over the continental shelf: High drag states over a small bank. *J. Geophys. Res.,* **106,** 4593–4611.

Shay, T. J., and M. C. Gregg, 1986: Convectively-driven turbulent mixing in the upper ocean. *J. Phys. Oceanogr.,* **16,** 1777–1798.

Skyllingstad, E. D., and D. W. Denbo, 1995: An ocean large eddy simulation of Langmuir circulations and convection in the surface mixed layer. *J. Geophys. Res.,* **100,** 8501–8522.

Soloviev, A., and B. Klinger, 2001: *Open Ocean Convection. Vol. 4, Encyclopedia of Ocean Sciences,* Academic Press, 2015–2022.

Stull, R. B., 1988: *An Introduction to Boundary Layer Meteorology.* Kluwer Academic, 666 pp.

Tennekes, H., and J. L. Lumley, 1972: *A First Course in Turbulence.* MIT Press, 300 pp.

Terray, E. A., M. A. Donelan, Y. C. Agrawal, W. M. Drennan, K. K. Kahma, and A. J. Williams III, 1996: Estimates of kinetic energy dissipation under breaking waves. *J. Phys. Oceanogr.,* **26,** 792–807.

Trowbridge, J. H., and S. J. Lentz, 1991: Asymmetric behavior of an oceanic boundary layer above a sloping bottom. *J. Phys. Oceanogr.,* **21,** 1171–1185.

Turner, J. S., 1973: *Buoyancy Effects in Fluids.* Cambridge University Press, 368 pp.

Weatherly, G. L., and P. J. Martin, 1978: On the structure and dynamics of the oceanic bottom boundary layer. *J. Fluid Mech.,* **36,** 289–307.